Monthly Notices of the ROYAL ASTRONOMICAL SOCIETY

MNRAS **459,** 1687–1697 (2016) doi:10.1093/mnras/stw716
Advance Access publication 2016 March 30

The VMC survey – XX. Identification of new Cepheids in the Small Magellanic Cloud

M. I. Moretti,[1,2,3★] G. Clementini,[1] V. Ripepi,[4] M. Marconi,[4] S. Rubele,[5,6] M.-R. L. Cioni,[7,8,9] T. Muraveva,[1] M. A. T. Groenewegen,[10] N. J. G. Cross,[11] V. D. Ivanov,[12,13] A. E. Piatti[14,15] and R. de Grijs[16,17,18]

[1]*INAF-Osservatorio Astronomico di Bologna, via Ranzani 1, I-40127 Bologna, Italy*
[2]*Scuola Normale Superiore di Pisa, piazza dei Cavalieri 7, I-56126 Pisa, Italy*
[3]*IAASARS, National Observatory of Athens, GR-15236 Penteli, Greece*
[4]*INAF-Osservatorio Astronomico di Capodimonte, via Moiariello 16, I-80131 Napoli, Italy*
[5]*INAF-Osservatorio Astronomico di Padova, vicolo dell'Osservatorio 5, I-35122 Padova, Italy*
[6]*Dipartimento di Fisica e Astronomia, Università di Padova, Vicolo dell'Osservatorio 2, I-35122 Padova, Italy*
[7]*Institut für Physik und Astronomie, Universität Potsdam, Karl-Liebknecht-Str. 24/25, D-14476 Potsdam, Germany*
[8]*Leibnitz-Institut für Astrophysik Potsdam, An der Sternwarte 16, D-14482 Potsdam, Germany*
[9]*School of Physics, Astronomy and Mathematics, University of Hertfordshire, Physics Astronomy and Mathematics, College Lane, Hatfield AL10 9AB, UK*
[10]*Royal Observatory of Belgium, Ringlaan 3, B-1180 Brussels, Belgium*
[11]*Wide-Field Astronomy Unit, Institute for Astronomy, School of Physics and Astronomy, University of Edinburgh, Royal Observatory, Blackford Hill, Edinburgh EH9 3HJ, UK*
[12]*European Southern Observatory, Ave. Alonso de Crdova 3107, Vitacura, Santiago, Chile*
[13]*European Southern Observatory, Karl-Schwarzschild-Str. 2, D-85748 Garching bei München, Germany*
[14]*Observatorio Astronómico, Universidad Nacional de Córdoba, Laprida 854, 5000 Córdoba, Argentina*
[15]*Consejo Nacional de Investigaciones Científicas y Técnicas, Av. Rivadavia 1917, C1033AAJ Buenos Aires, Argentina*
[16]*Kavli Institute for Astronomy and Astrophysics, Peking University, Yi He Yuan Lu 5, Hai Dian District, Beijing 100871, China*
[17]*Department of Astronomy, Peking University, Yi He Yuan Lu 5, Hai Dian District, Beijing 100871, China*
[18]*International Space Science Institute-Beijing, 1 Nanertiao, Zhongguancun, Hai Dian District, Beijing 100190, China*

Accepted 2016 March 23. Received 2016 March 22; in original form 2015 October 27

ABSTRACT

We present K_s-band light curves for 299 Cepheids in the Small Magellanic Cloud (SMC) of which 288 are new discoveries that we have identified using multi-epoch near-infrared photometry obtained by the VISTA survey of the Magellanic Clouds system (VMC). The new Cepheids have periods in the range from 0.34 to 9.1 d and cover the magnitude interval $12.9 \leq \langle K_s \rangle \leq 17.6$ mag. Our method was developed using variable stars previously identified by the optical microlensing survey OGLE. We focus on searching new Cepheids in external regions of the SMC for which complete VMC K_s-band observations are available and no comprehensive identification of different types of variable stars from other surveys exists yet.

Key words: methods: data analysis – surveys – stars: variables: Cepheids – Magellanic Clouds.

1 INTRODUCTION

The Visual and Infrared survey Telescope for Astronomy (VISTA; Emerson, McPherson & Sutherland 2006) survey of the Magellanic Clouds system (VMC; Cioni et al. 2011, 2013) is collecting Y, J, K_s photometry[1] down to $Y = 21.9$ mag, $J = 22.0$ mag, $K_s = 21.5$ mag (5σ level on the stacked images) for sources in the Large Magellanic Cloud (LMC), the Small Magellanic Cloud (SMC), the Bridge connecting them and a small part of the Magellanic Stream. The VMC images are processed by the Cambridge Astronomical Survey Unit (CASU;[2] Lewis, Irwin & Bunclark 2010) through the VISTA Data Flow System pipeline that performs aperture photometry of the images. The reduced data are then further processed by the Wide Field Astronomy Unit (WFAU)[3] in Edinburgh where the single epochs are stacked and catalogued in the VISTA Science

★ E-mail: mariaidamoretti@noa.gr
[1] The VMC system is similar to the Vega magnitude system (see, e.g. Rubele et al. 2012).
[2] http://casu.ast.cam.ac.uk/
[3] http://horus.roe.ac.uk/vsa

© 2016 The Authors
Published by Oxford University Press on behalf of the Royal Astronomical Society

Downloaded from https://academic.oup.com/mnras/article/459/2/1687/2595101 by guest on 28 November 2020

Archive (VSA; Cross et al. 2012). As of 2016 January, the VMC survey observations are 74 per cent complete, with specific completion levels of 62 per cent, 95 per cent, 95 per cent and 100 per cent for the LMC, the SMC, the Bridge and the Stream, respectively. One of the main aims of the VMC survey is to study the structure of the whole Magellanic system using different distance indicators. Among them, most notably, are primary standard candles such as the Cepheids and the RR Lyrae (RRLYR) stars, for which VMC is obtaining K_s-band light curves with 13 (or more) individual epochs, with most epochs reaching a depth of $K_s = 19.3$ mag (5σ level). The significantly reduced amplitude of these pulsating variables in the near-infrared, with respect to the optical bands, along with the multi-epoch cadence of the VMC K_s-band observations, allows us to infer accurate mean K_s magnitudes. Furthermore, the near-infrared period–luminosity (PL) relations are intrinsically much narrower than the corresponding optical relations and less affected by systematic uncertainties in reddening and metal content (Caputo, Marconi & Musella 2000). For these reasons the VMC data are very well suited to construct PL relations with a high level of precision and accuracy (e.g. Ripepi et al. 2012a,b, 2014, 2015; Muraveva et al. 2015). Conversely, the smaller amplitudes compared to optical bands make it more difficult to identify these variables from near-infrared data alone. In VMC, most of the information (identification, period, variability type, etc.) needed to fold the *Y*-, *J*-, K_s-band light curves and derive average *Y*, *J*, K_s magnitudes for the variable stars are taken from the catalogues of Magellanic Cloud variables produced by large microlensing optical surveys such as MACHO (Alcock et al. 2000), EROS (Tisserand et al. 2007) and OGLE (Soszyński et al. 2008a) that were conducted in the last two decades to search for baryonic dark matter in the Milky Way. As described in Udalski et al. (2015), the observations of the fourth phase of the OGLE project (hereinafter, OGLE IV) have been successfully run over the last five years. First results have been published in Soszyński et al. (2012, South Ecliptic Pole region), Kozłowski et al. (2013, Magellanic Bridge) and Soszyński et al. (2015a, anomalous Cepheids).[4] However, as we are writing this paper, none of the available optical catalogues cover the field of view of VMC entirely (see fig. 4 of Moretti et al. 2014). There are external regions in both the LMC and SMC, and the whole Bridge area where a comprehensive census of all types of variable stars is still missing. On the other hand, in VMC each field is observed in the K_s band at least 13 times (Cioni et al. 2011): 11 times with an exposure of 750 s (deep observations, hereafter) and twice with shorter exposures of 375 s each (shallow observations, hereafter) obtained over more than 1-yr time-span. Furthermore, the VSA provides a list of flags related to the analysis of the light curves of each VMC source (Cross et al. 2012) that can be used to identify variable sources. In this paper we show that, in spite of the small amplitudes in the near-infrared, pulsating variable stars can be effectively detected from the VMC data if a proper analysis is performed. Specifically, we combine the information from (i) the ($J - K_s$, K_s) colour–magnitude and the ($Y - J$, $Y - K_s$) colour–colour diagrams, (ii) the analysis of the K_s-band light curves, (iii) the PL relations and (iv) the VSA flags, to devise a procedure and detect variable stars in the external regions of the Magellanic system using only the VMC data.

[4] During the revision phase of this manuscript, results on classical Cepheids in the Magellanic Clouds have been published by Soszyński et al. (2015b). See Section 4.

This paper is organized as follows. The reliability of the VSA flags in detecting variable stars is presented in Section 2. Section 3 describes the method to identify variable stars in the SMC where information is available from the OGLE III survey. In Section 4 we apply our method to identify classical Cepheids (CCs) in external regions of the SMC where the VMC observations are complete and no other CC variable star catalogue is currently available. Our results are summarized in Section 5.

2 IDENTIFICATION OF VARIABLE STARS USING THE VSA FLAGS

We have tested the ability of the VSA in identifying variable stars based solely on the VMC data in three most external and completely observed tiles in the LMC, namely tile LMC 6_8, 7_3 and 8_8. The upper portion of Table 1 provides centre coordinates of these three LMC tiles, together with information related to their observations. We specifically selected these three tiles because they contain a large number of variable stars of different types and are located in external fields of the LMC with similar level of crowding as in the regions where we currently have VMC data, but there is no coverage by the optical surveys. We first cross-matched the OGLE catalogues (Soszyński et al. 2008a,b, 2009a,b, 2012; Poleski et al. 2010; Graczyk et al. 2011) of variable stars in these fields against the VMC catalogue of the corresponding three tiles. We adopted a pairing radius of 0.5 arcsec in order to maximize the reliability of the matching procedure as discussed in Ripepi et al. (2015). There are 7206 variable stars in common between the two catalogues; in particular we have 94 δ Scuti (DSCT) stars, 1071 RRLYR stars, 1521 Eclipsing binaries (ECL), 217 CCs, 4289 Long Period Variables (LPVs, among which are 83 Mira, 3626 OGLE Small Amplitude Red Giants – OSARGs – and 580 SemiRegular Variables – SRVs), six Type II Cepheids (T2Ceps) and eight Anomalous Cepheids (ACs). For all of them we investigated the variability classification provided by the VSA; this is summarized by the *'Variability Class'* parameter which is the result of the analysis performed by the WFAU team on the *Y*-, *J*- and K_s-band light curves of the sources. *'Variability Class'* is either 1 or 0, whether or not the object is classified as variable (Cross et al. 2009, 2012). Table 2 compares the number of OGLE variable stars cross-matched with VMC sources in the aforementioned tiles and the number of them classified as variables by the VSA (*VariableClass* = 1).

The effectiveness of the VSA in selecting variable stars depends on the mean magnitude, period and amplitude of the light variation and, in turn, on the type of variability. Indeed, according to the numbers in Table 2 the type of variable stars most easily classified as such by the VSA are the LPV-Mira, ACs, LPV-SRV, T2Ceps and CCs. Note that the sample of T2Ceps and of ACs are not statistically representative. In this paper we focus on the detection of Cepheids, CCs in particular, because they are numerous and will give us a very good statistical sample to work with. We leave for a future paper the analysis of other types of variables. CCs typically have single-epoch photometric errors in the K_s band of about 0.01 mag (Ripepi et al. 2012b; Moretti et al. 2014), typical K_s amplitudes between 0.05 and 0.38 mag and periods between ∼0.5 d and tens of days. The search for CCs was performed in regions of the Magellanic system where we expect this kind of variable stars to be present and the VMC observations are complete, but for which no optical data are currently available. In particular, we focused on the external regions of the SMC (see Section 4).

Downloaded from https://academic.oup.com/mnras/article/459/2/1687/2595101 by guest on 28 November 2020

Table 1. Information on the K_s-band photometry of the VMC tiles analysed in this paper. Column 1: field and tile number; column 2: right ascension (RA, J2000); column 3: declination (Dec, J2000); column 4: position angle; column 5: number of K_s observations; columns 6,7: dates of the first and last observations expressed in yy-mm-dd format; column 8: time interval (T.I.) between first and last observations; column 9: airmass; column 10: full width at half-maximum (FWHM); column 11: ellipticity; column 12: limiting magnitude. Reported values of airmass, FWHM, ellipticity and limiting magnitude are averages over all nights. They are indicated with their respective standard deviations. The number of epochs (N_{K_s}) includes both shallow and deep observations (see text for details).

Tile	α ($^h:^m:^s$)	δ ($^\circ:':''$)	ϕ (deg)	N_{K_s}	1st epoch	Last epoch	T. I. (d)	Airmass	FWHM	e	LimMag (mag)
LMC 6_8	06:02:21.984	−69:14:42.360	−83.7904	15	11-02-23	14-04-16	1148	1.49 ± 0.04	0.96 ± 0.19	0.06 ± 0.01	19.30 ± 0.24
LMC 7_3	05:02:55.200	−67:42:14.760	−97.7044	16	11-01-12	13-03-04	782	1.44 ± 0.05	0.95 ± 0.10	0.06 ± 0.02	19.23 ± 0.19
LMC 8_8	05:59:23.136	−66:20:28.680	−84.4802	16	09-11-14	10-11-26	377	1.39 ± 0.05	0.93 ± 0.11	0.06 ± 0.02	19.36 ± 0.27
SMC 3_1	00:02:39.912	−73:53:31.920	−11.3123	16	12-08-21	14-07-01	679	1.60 ± 0.05	1.01 ± 0.15	0.05 ± 0.01	19.38 ± 0.16
SMC 3_3	00:44:55.896	−74:12:42.120	−1.2120	18	11-08-03	12-09-05	399	1.62 ± 0.04	1.02 ± 0.10	0.07 ± 0.02	19.35 ± 0.15
SMC 3_5	01:27:30.816	−74:00:49.320	+8.9671	16	11-07-29	12-10-07	436	1.58 ± 0.06	1.02 ± 0.15	0.06 ± 0.01	19.34 ± 0.22
SMC 4_2	00:25:14.088	−73:01:47.640	−5.9198	15	12-10-18	14-06-23	606	1.57 ± 0.06	0.94 ± 0.08	0.05 ± 0.01	19.29 ± 0.21
SMC 4_3	00:45:14.688	−73:07:11.280	−1.1369	16	11-08-29	13-08-18	720	1.56 ± 0.05	0.92 ± 0.10	0.07 ± 0.01	19.27 ± 0.17
SMC 4_4	01:05:19.272	−73:05:15.360	+3.6627	15	12-09-25	14-07-14	648	1.56 ± 0.06	0.87 ± 0.06	0.07 ± 0.02	19.27 ± 0.16
SMC 4_5	01:25:11.016	−72:56:02.040	+8.4087	18	11-08-29	13-11-25	819	1.56 ± 0.06	0.92 ± 0.17	0.06 ± 0.01	19.42 ± 0.19
SMC 5_2	00:26:41.688	−71:56:35.880	−5.5717	17	11-06-09	12-11-10	520	1.53 ± 0.06	0.99 ± 0.18	0.07 ± 0.01	19.24 ± 0.27
SMC 5_3	00:44:49.032	−72:01:36.120	−1.2392	19	12-10-04	14-08-08	673	1.54 ± 0.07	0.95 ± 0.12	0.06 ± 0.01	19.31 ± 0.15
SMC 5_4	01:04:26.112	−71:59:51.000	+3.4514	18	10-10-26	12-10-23	728	1.58 ± 0.08	0.92 ± 0.11	0.07 ± 0.01	19.35 ± 0.15
SMC 5_6	01:41:28.800	−71:35:47.040	12.3004	18	11-09-30	14-09-11	1077	1.58±0.08	1.0±0.2	0.05±0.01	19.15 ± 0.65
SMC 6_3	00:45:48.768	−70:56:08.160	−1.0016	14	11-08-20	13-11-06	809	1.52 ± 0.06	0.95 ± 0.12	0.05 ± 0.01	19.39 ± 0.22
SMC 6_5	01:21:22.488	−70:46:10.920	+7.5039	14	11-09-06	13-10-18	773	1.49 ± 0.03	0.97 ± 0.17	0.05 ± 0.01	19.42 ± 0.17

Table 2. VSA classification of variable stars within VMC tiles LMC 6_8, 7_3 and 8_8. Column 1: type of variable stars; column 2: number of OGLE III stars with a VMC counterpart within 0.5 arcsec; column 3: number of stars classified as variables by the VSA; column 4: percentage value. See text for details.

Type	N_{OGLE}	N_{VSA}	N per cent
DSCT	94	1	1 per cent
RRLYR	1071	28	3 per cent
ECL	1521	132	9 per cent
LPV-OSARG	3626	576	16 per cent
CC	217	137	63 per cent
T2Cep	6	4	67 per cent
LPV-SRV	580	477	82 per cent
AC	8	7	87 per cent
LPV-Mira	83	75	90 per cent

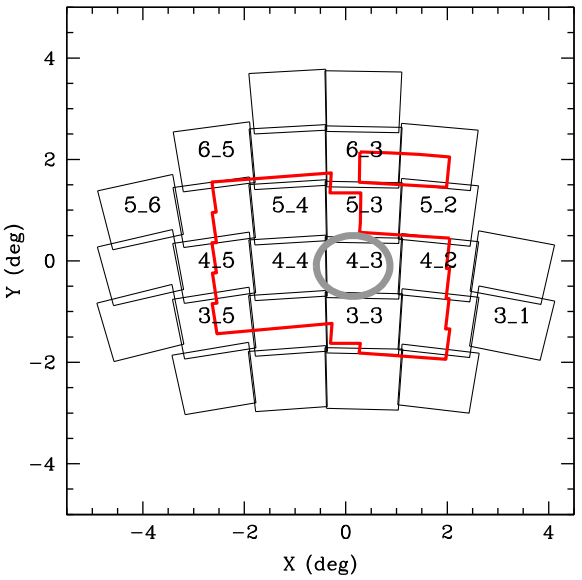

Figure 1. Celestial distribution of OGLE III footprint (red contours) and VMC tiles (black rectangles) in the SMC area. X and Y are defined as in van der Marel & Cioni (2001) with $\alpha_0 = 12.5$ deg and $\delta_0 = -73.0$ deg. Tiles analysed in this work are labelled with their VMC IDs. The grey oval shows the area containing the peak density of the SMC CCs which was avoided in the present analysis.

3 DEFINING THE METHOD TO DETECT CLASSICAL CEPHEIDS

In order to specifically optimize the detection of CCs, we first analysed the properties of the VMC data for variable stars in the SMC classified as CCs by OGLE III (Soszyński et al. 2010a). These authors identified 4630 CCs in the SMC, of which 2626 are fundamental-mode (F), 1644 are first-overtone (1O), 83 are second-overtone (2O), 274 are double-mode (59 F/1O and 215 1O/2O) and three are triple-mode CCs. The mean I-band magnitude of these CCs ranges from ∼10 mag to ∼19 mag, with two major peaks at I ∼16.8 mag and ∼15.8 mag. We have used the OGLE III coordinates of the SMC CCs as reference in the following analysis. Fig. 1 shows the distribution of the OGLE III footprint (red contours) and the VMC tiles (black rectangles) in the SMC area. The SMC tiles analysed in this work are the ones for which the VMC observations were completed before 2014 September 30. They are tiles SMC 3_3, 3_5, 4_2, 4_3, 4_4, 4_5, 5_2, 5_3, 5_4, 6_3 and 6_5, labelled with their IDs in Fig. 1. The lower portion of Table 1 lists centre coordinates and observation properties for all of them. OGLE III observations cover the most central and crowded regions of the SMC. In particular, the peak in stellar density (see fig. 1 of Rubele et al. 2015) and CC density (see right-hand panel of fig. 18 in Moretti et al. 2014) in the SMC occurs in an area centred at coordinates RA = 12 deg, Dec = −73.1 deg and radius of 2 deg in RA and 0.5 deg in Dec. This region, marked by a grey oval in Fig. 1, mainly covers the tile SMC 4_3 and contains 1695 of the 4630 CCs identified by the OGLE III survey in the SMC. However, as we aim at fine-tuning our procedures to identify new

Downloaded from https://academic.oup.com/mnras/article/459/2/1687/2595101 by guest on 28 November 2020

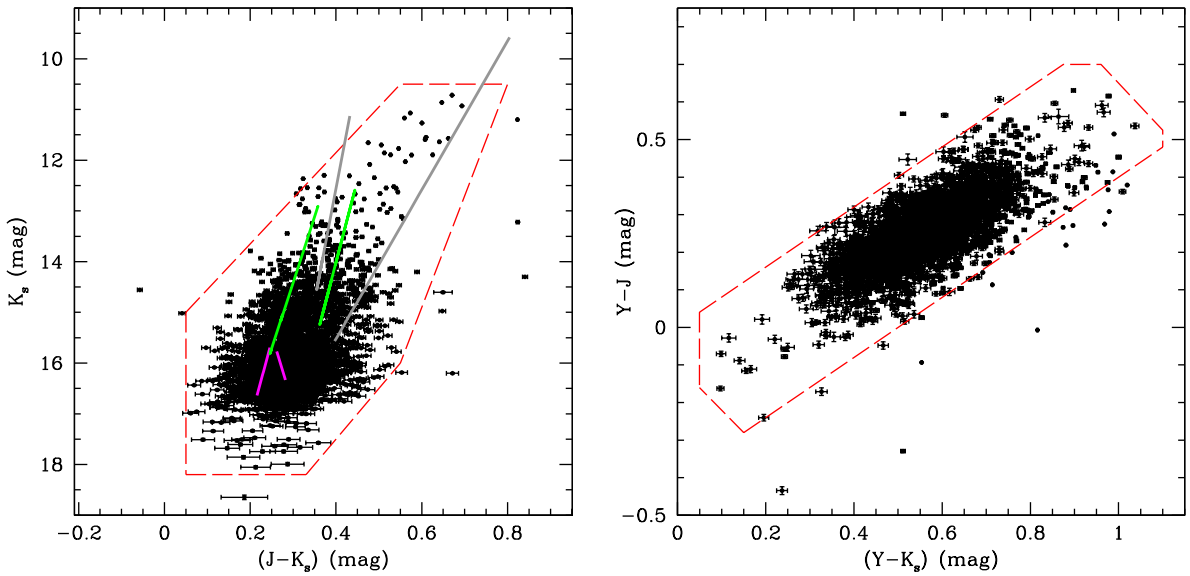

Figure 2. Left: distribution of known SMC CCs in the ($J - K_s$, K_s) colour–magnitude diagram. Grey, green and magenta solid lines represent the theoretical blue and red edges of the CC ISs for F, 1O and 2O pulsation modes, respectively. Right: same as the left-hand panel but in the ($Y - J$, $Y - K_s$) colour–colour diagram. In both panels, red dashed contours indicate the boundaries of the region that will be used to select candidate CCs in the external part of the SMC. See Section 3 for details.

SMC CCs outside the OGLE III field (see Section 4), we considered in the following analysis only CCs lying in the external portions of the OGLE III footprint, where the level of crowding and reddening is similar to what we found in the regions which currently have only VMC data (see Fig. 1). Specifically, we considered 2935 CCs located outside the oval shape in Fig. 1. By matching the OGLE III and VMC catalogues, using a pairing radius of 0.5 arcsec we obtained a sample of 2411 CCs that have VMC K_s-band light curves. Increasing the paring radius to 1.0 arcsec would result in increasing by about 1 per cent the number of misidentifications. Conversely, reducing the paring radius to 0.1 arcsec, would result in losing about 10 per cent of the cross-matched sources. On the other hand, the reliability of our cross-identifications and, in turn, of the value adopted for the paring radius, is specifically assessed by folding the VMC K_s-band light curves according to the corresponding OGLE III periods (e.g. Ripepi et al. 2015). These CCs lie in the tiles (see Fig. 1): SMC 3_3, 3_5, 4_2, 4_3 and 4_4 (excluding sources inside the oval grey contour), 4_5, 5_2 (two sources), 5_3, 5_4, 6_3 (four sources) and 6_5 (two sources).

3.1 Selection based on the colour–magnitude and colour–colour diagrams

We used the sample of 2411 OGLE III CCs described in the previous section as a reference to define the range in VMC colours and magnitudes in which the SMC CCs lie. Fig. 2 shows the distribution of such stars in the ($J - K_s$, K_s) colour–magnitude diagram. We have highlighted with red dashed contours the region that we will use to select CC candidates. We note that 2365 of the 2411 reference CCs (corresponding to 98 per cent of the sample) have $\langle K_s \rangle < 17.0$ mag and only 2 per cent of the population have fainter magnitudes. Specifically, 45 stars have $17.0 \leq \langle K_s \rangle \leq 18.2$ mag and only one CC is as faint as $\langle K_s \rangle = 18.6$ mag. We have also reported in Fig. 2 the theoretical instability strips (ISs) for CCs with metallicity $Z = 0.004$ and helium abundance $Y = 0.25$ taken from Bono, Castellani & Marconi (2000), Bono, Caputo & Marconi (2001a) and Bono et al. (2001b). These values of Z and Y are appropriate for the SMC CCs. To transform the theoretical IS edges to the observational plane we adopted the static model atmospheres by Castelli, Gratton & Kurucz (1997a,b), an absorption $A_V = 0.1$ mag (Haschke, Grebel & Duffau 2011) and a distance modulus of 19.0 mag, computed as the weighted average of the CC results in table 1 of Haschke, Grebel & Duffau (2012).[5]

Specifically, we have plotted in Fig. 2 the blue and red edges of the IS for CCs of different pulsation modes: F (grey lines), 1O (green lines) and 2O (magenta lines). For magnitudes brighter than 14 mag, there is reasonably good agreement, within the errors, between theoretical and observed ISs, suggesting that the sample of CCs we are using as reference (Soszyński et al. 2010a), once matched with the VMC data, represents the ranges in K_s magnitude and $J-K_s$ colour covered by the SMC CCs very well. A number of reference CCs, especially at magnitudes fainter than $K_s \sim 14$ mag, are found beyond the boundaries of the theoretical ISs, both at bluer and redder colours. This is likely caused by metallicity, differential reddening issues and by the poor sampling of their VMC J-band light curves. Indeed, the same theoretical ISs are in much better agreement with other observational samples, including Magellanic Cepheids, where light curves are better sampled in colour (e.g. Bono et al. 1999; Marconi, Musella & Fiorentino 2005). We also compared the colour–magnitude distribution for sources with more than 10 data points in the J band (about 10 per cent of our sample) using the $J-K_s$ colours obtained after analysing both the J and K_s-band light curves with a custom template-fitting procedure (Ripepi et al. 2015, 2016). We obtained a relatively more compact distribution, confirming that the poor sampling of the VMC J-band light curves is one of the possible issues.

The right-hand panel of Fig. 2 shows the distribution of these CCs in the $Y - J$, $Y - K_s$ colour–colour diagram. As in Fig. 2, we have highlighted with red dashed contours the region that we will use in Section 4 to select CC candidates.

[5] This method applied to the CC results listed in table 2 of de Grijs & Bono (2015) leads exactly to the same distance modulus value.

Downloaded from https://academic.oup.com/mnras/article/459/2/1687/2595101 by guest on 28 November 2020

3.2 Analysis of the light curves

OGLE III periods of the reference CCs range between 0.25 and 208 d. The vast majority of the reference CCs (2240 sources) have $P < 5$ d, 109 sources have $5 \leq P < 10$ d, 60 have $10 \leq P < 75$ d and only two sources have $P \geq 75$ d. Specifically, these two sources have $P_{\rm OGLE} = 128.2$ and 208.8 d; although their $K_{\rm s}$-band photometry ($K_{\rm s} \sim 11$ mag) should not be saturated, they are fainter than expected according to the $K_{\rm s}$-band PL relation, especially the last one. The same feature occurs in the *I*-band OGLE data. Despite the fact that their images do not show any clear problem, their folded $K_{\rm s}$-band light curves are very noisy without a clear shape; for these reasons we decided to discard them and focus on the sources with *P* lower than 80 d.

We analysed the $K_{\rm s}$-band light curves and derived the period of the reference CCs from the $K_{\rm s}$ time series data alone, ignoring OGLE III information on the period. We used all available VMC epochs to study the light curves including observations obtained during nights with sky conditions (i.e. seeing and ellipticity) that exceeded the VMC requirements (Cioni et al. 2011), since our fitting procedure is able to handle lower accuracy data (see, e.g., Ripepi et al. 2015 and references therein). The resulting light curves have a number of data points that range from 7 to 60. We checked the images of some CCs with a few epochs and found that often these sources are contaminated by very bright companions.

Periods were derived using the program 'Significance Spectrum' (SigSpec; Reegen 2004, 2007, 2011). SigSpec is a method specifically developed for detecting and characterizing periodic signals in noisy data. While most period search analyses explore only the Fourier amplitude, through the power spectrum, ignoring phase information, SigSpec is based on the definition of a quantity called *spectral significance* for a time series, a function of Fourier phase and amplitude. The *spectral significance* quantity conveys more information than does the conventional amplitude spectrum alone, and appears to simplify statistical issues as well as the interpretation of phase information.

We ran SigSpec on the VMC $K_{\rm s}$-band time series adopting a lower period of 0.25 d, an upper period of 80 d and weighting by the $K_{\rm s}$ single-epoch errors. The rms of the light-curve analysis typically ranged from 0.002 to 0.15 mag, (with a few extreme values as large as 0.3 mag) and a median value of 0.015 mag. The median value of the *spectral significance* is ~ 3.0 with a standard deviation of 0.9, and minimum and maximum values of 0.9 and 7.0 (see also discussion at the end of Section 3.3). Fig. 3 shows the comparison between the OGLE III periods and the periods we derived for the reference CCs running SigSpec on the $K_{\rm s}$ time series data. For 54 per cent of the sources (1302 stars) the two periods are in good agreement, the difference being smaller than 0.02 d. On the other hand, for some stars the period found by SigSpec ($P_{\rm SigSpec}$) is definitely shorter than that published by the OGLE team. In particular, about 800 sources have $\Delta P = P_{\rm OGLE}$ (where $\Delta P = P_{\rm OGLE} - P_{\rm SigSpec}$) because their $P_{\rm SigSpec}$ is near zero (see Fig. 3). This is probably due to alias problems in the case of sources with period shorter than a few days and to saturation of the $K_{\rm s}$ time series for stars with longer period. Conversely, there are about 150 stars for which $P_{\rm SigSpec}$ is definitely longer than $P_{\rm OGLE}$ and hence ΔP assumes large negative values (see Fig. 3). This might be due to faintness and hence poor quality of the $K_{\rm s}$ light curves of these stars that affect the period search procedure. We also checked if there is any dependence of ΔP on the amplitude of the light curves, but did not find any. We do not have an estimate of the error on $P_{\rm SigSpec}$ for each star but, assuming the OGLE as the correct one, we can use as an estimate of the $P_{\rm SigSpec}$ error the median value of ΔP, that is 0.002 d.

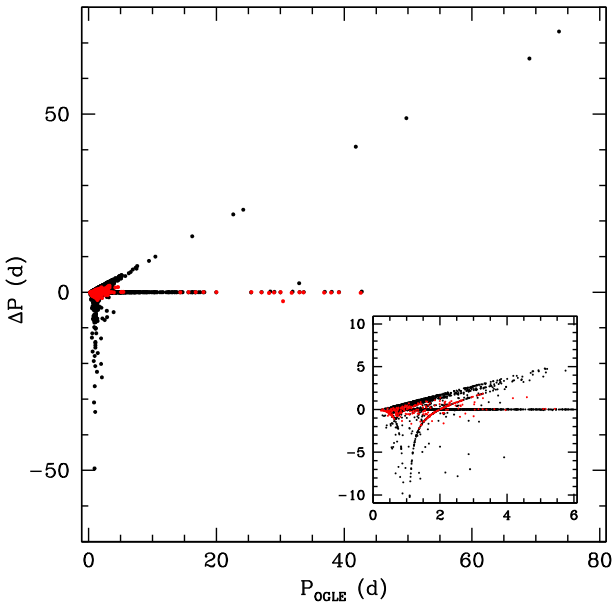

Figure 3. Distribution of $\Delta P = P_{\rm OGLE} - P_{\rm SigSpec}$ versus $P_{\rm OGLE}$. Shown in the inset is an enlargement of the short period region. Red points indicate stars within 3σ from the PL relations but with ΔP larger than 0.02 d. See text and Fig. 4 for details.

As an additional test, we performed an analysis of the $K_{\rm s}$ light curves using a different period search program, FNPEAKS (Kurtz 1985). We adopted the same limits (0.25–80 d) for the period and a frequency step of 0.0001 s^{-1}. For 29 per cent of the stars there is good agreement between the OGLE IIII and the FNPEAKS periods: $|\Delta P| \leq 0.02$ d. FNPEAKS does not allow us to weight by the error of the single epoch magnitudes; this probably explains the lower percentage of periods recovered within 0.02 d with respect to SigSpec (54 per cent). We also checked the *P* versus ΔP plot, that is the counterpart of Fig. 3. The shape of the $\Delta P = P_{\rm OGLE} - P_{\rm FNPEAKS}$ versus $P_{\rm OGLE}$ is very similar to Fig. 3, hence confirming that FNPEAKS and SigSpec find consistent results; however, SigSpec appears to be more efficient. In the analysis described in Section 4 we will thus adopt SigSpec to estimate the period of the candidate variable stars.

3.3 Selection based on the PL relation

Fig. 4 shows the $K_{\rm s}$-band PL plane obtained for the 2411 reference CCs using for the period values derived with the SigSpec analysis and for the $K_{\rm s}$ average magnitude values available from the VSA. Red solid lines show the PL fits obtained for F and 1O mode CCs, using the periods from OGLE III; red dashed lines show the corresponding 3σ boundaries for 1O (upper dashed line) and F (lower dashed line) CCs, respectively. As expected, Cepheids with a good SigSpec estimate of the period ($|\Delta P| \leq 0.02$ d, black points) lie near the PLs defined using the OGLE III periods. Specifically, there are 1589 objects lying within 3σ from the PLs, corresponding to 66 per cent of the original sample.[6] This number includes 1304 stars with $|\Delta P| \leq 0.02$ d (black points) and 285 sources with $|\Delta P|$ larger than 0.02 d (grey points). These 285 sources are marked by red points in the ΔP versus $P_{\rm OGLE}$ distribution shown in Fig. 3. The bulk of the distribution has $|\Delta P| \leq 1$ d (253 objects), and only a

[6] This number reduces to 1139, corresponding to 47 per cent of the original sample, if the periods obtained with FNPEAKS are used instead.

Downloaded from https://academic.oup.com/mnras/article/459/2/1687/2595101 by guest on 28 November 2020

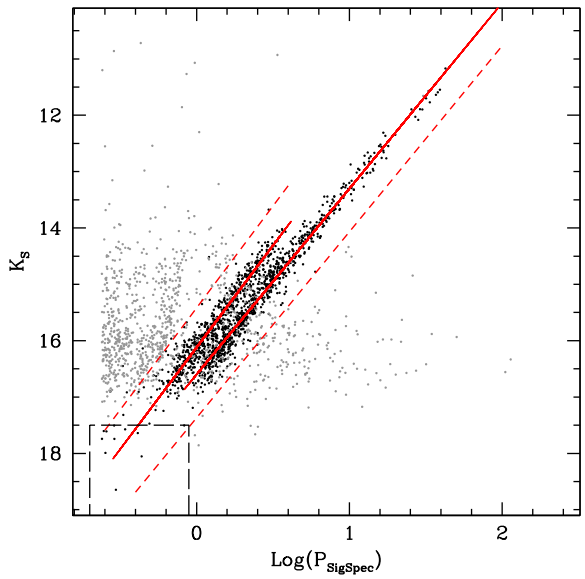

Figure 4. Distribution of known SMC CCs in the period–K_s-band luminosity plane using for the period values derived from the analysis of the K_s-band light curves. Red solid lines show the PL relations for F (right) and 1O (left) CCs derived using the OGLE III periods. Red dashed lines represent 3σ boundaries of the 1O (upper line) and F (lower line) PLs, respectively. Black and grey dots show stars with $|\Delta P| \leq 0.02$ d and $|\Delta P| > 0.02$ d, respectively. A black dashed box marks the region populated by RR Lyrae stars. See Section 4.1 for details.

few sources (32 stars) have ΔP values larger than $\pm$ 1 d and up to 2.5 d.

Stars within the 3σ from the PLs, show an average *significance* (see Section 3.2) of 3.4 with minimum and maximum values of 1.8 and 7.0, respectively. We checked the position of these stars on the PL according to their *significance* value and noted that several stars with *significance* value between 1.8 and 2.0 lie within 2σ from the PLs. Hence, in the following analysis we will retain only sources with *significance* larger than 1.7 (Section 4). We will also take into account the possible contamination by other types of variable stars. In particular, the RRLYR stars follow a PL_{K_s} relation that, although different, partially overlaps with the PL_{K_s} relation of CCs. A black dashed box schematically shows the locus of the SMC RRLYR stars in the K_s-band PL plane in Fig. 4. This issue will be discussed in more detail in Section 4.1.

3.4 VSA flags

The VSA provides several flags describing the quality of the light curve of each VMC source. A complete explanation of these parameters is provided in Cross et al. (2012) and on the VSA web page.[7] Here we briefly summarize the properties that are relevant for the present study. The VSA classifies sources according to their nature by the *mergedClass* parameter within the *vmcSource* table, containing the information about the sources extracted from the stacked images. Specifically, the association between parameter value and physical nature of the source is as follows: 1 = galaxy, 0 = noise, -1 = stellar, -2 = probable star, -3 = probable galaxy, -9 = saturated source. The *KsppErrBits* parameter encodes quality issues associated with a given K_s-band detection within the vmcSource table. Its value is zero for a detection without quality issues and grows according to the severity of the issue. In particular to include sources with only minor K_s-band quality issues the user can filter as *KsppErrBits* <256.

We used the VSA flags to select among our sample of 2411 reference CCs only stars with at least 10 data points (this corresponds to 2407 of the 2411 sources), that are classified as stars or probable stars by the VSA (*mergedClass* = -1 or -2), as variables (*VarClass* = 1) and that do not exhibit any severe quality issues (*KsppErrBits* <256), thus ending up with a total of 1445 sources. This corresponds to 60 per cent of our original sample. 500 of the sources that the VSA classifies as non-variable sources (*VarClass* = 0) perfectly lie within the 3σ limits from the PLs. Hence, the VSA flags, although useful for a first selection of variable sources, need to be fine-tuned (see, e.g., Ferreira Lopes & Cross 2016) to increase their capability to detect bona fide variable stars. In the next section we will use the VSA flags to corroborate our identification of new SMC CCs based on the colour–magnitude and colour–colour diagrams and PL selections described in the previous sections.

In conclusion, to identify CCs from the VMC K_s-band time series data we will

(i) first select candidate variables by applying the colour–magnitude and colour–colour diagram cuts described in Section 3.1,
(ii) analyse with SigSpec the light curves of the candidate variables to determine their periods (see Section 3.2),
(iii) consider as best candidates the stars falling within 3σ from the PLs defined as described in Section 3.3 and
(iv) investigate the VSA flags.

In this way, following a visual inspection of the light curves to identify bona fide CCs, we should be able to identify 66 per cent of the CCs that populate the external areas of the SMC analysed in the next section.

4 DETECTION OF CLASSICAL CEPHEIDS IN THE EXTERNAL REGIONS OF THE SMC

We have applied the methods described in Section 3 to look for CCs in all regions of the SMC where we currently have complete VMC data, but where no optical comprehensive catalogue of variable stars is available yet. Fig. 5 shows the portion of sky we have analysed with the different VMC tiles labelled in Fig. 1 (see also Table 1). We specifically considered only regions outside the OGLE III footprint (red solid lines) and also discarded the region studied by Weldrake et al. (2004; empty area within tile SMC 5_2 at $X \sim 2$, $Y \sim 1$), who provided a comprehensive catalogue of variable stars in the field of the Galactic globular cluster 47 Tucanae. In particular, we first selected our candidates in the aforementioned VMC tiles, and then discarded sources lying in the region that overlaps with the OGLE III and Weldrake et al. (2004) fields. The sources were then further selected using the colour–magnitude and colour–colour diagrams, as described in Section 3.1, yielding 19 938 candidate CCs, that are plotted as black points in Fig. 5.

Rubele et al. (2015) estimated the star formation history (SFH) in these regions of the SMC. By comparing the best-fitting SFH models with the theoretical CC ISs for $Z = 0.004$ and $Y = 0.25$ we predict a few hundreds CCs to populate the area under investigation. Hence, clearly, only a few percent of our 19 938 CC candidates are bona fide CCs. For 18 090 of these sources the VSA provides K_s-band light curves with at least 10 data points, we analysed them with SigSpec and defined their period following the procedure described in Section 3.2. Furthermore, we derived average K_s magnitudes

[7] http://horus.roe.ac.uk/vsa

Downloaded from https://academic.oup.com/mnras/article/459/2/1687/2595101 by guest on 28 November 2020

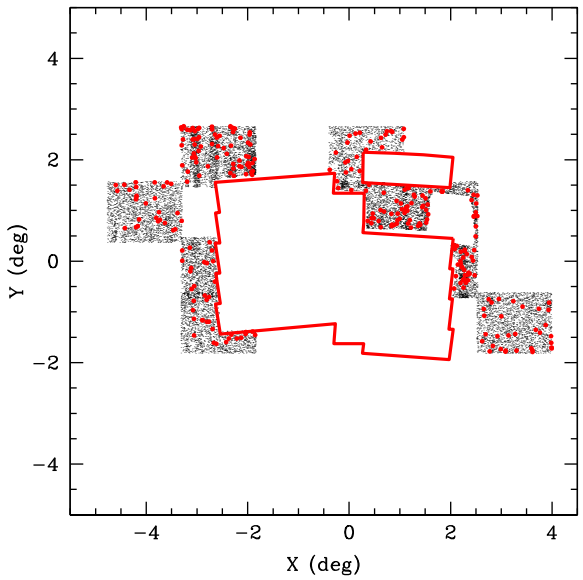

Figure 5. Spatial distribution of the SMC CC candidates (black points) selected using the tools described in Section 3. X and Y, the red contours and the VMC tiles are defined as in Fig. 1. The white area within tile SMC 5_2 at $X \sim 2$, $Y \sim 1$ corresponds to the 47 Tucanae field analysed by Weldrake et al. (2004). Sources that we confirm to be bona fide new Cepheids are marked by red filled circles (see text for details).

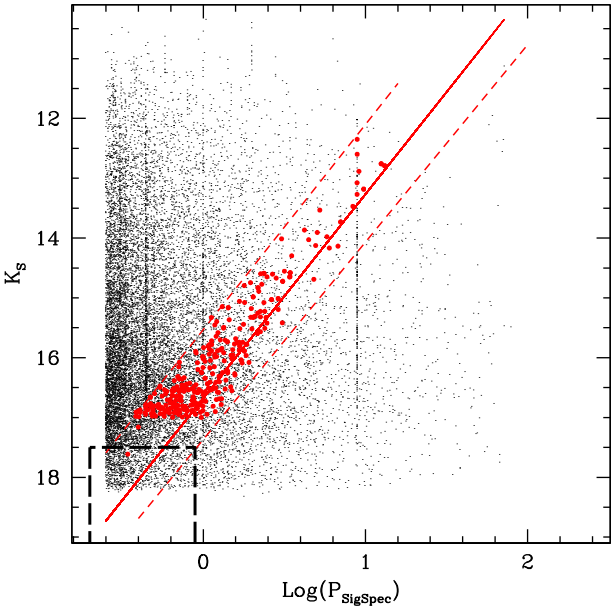

Figure 6. Distribution of the 18 090 candidate CCs (black points) in the period–K_s-band luminosity plane. Red solid lines show the PL relations and their 3σ boundaries (red dashed lines) defined by the OGLE III SMC CCs. A black dashed box highlights the region occupied by the SMC RR Lyrae stars. Red filled circles mark bona fide CCs identified in the present study. Their K_s-band light curves are shown in Fig. 7.

and K_s-band amplitudes (AmpK_s) analysing the light curves with an automatic template-fitting procedure specifically developed for the analysis of the K_s-band light curves of the SMC CCs (Ripepi et al. 2016). We then used the periods derived with SigSpec and the average K_s magnitudes computed as described above to plot the sources in the period–K_s luminosity plane shown in Fig. 6. We have also plotted in this figure the 3σ boundaries of the K_s-band PL relations defined by the OGLE III SMC CCs (see Section 3.3). Excluding objects more than 3σ away from the F and 1O mode PL relations the sample reduces to 4817 sources.

We further selected the sample using the parameters of the template-fitting procedure. A comprehensive description of this procedure and of its parameters is provided by Ripepi et al. (2016). Here we simply note that we used the parameter G, which gives an estimate of the goodness of the fit by weighting the residuals of the fit (rms) with the number of data points rejected (outliers) from the fitting procedure. The first term of G tends to favour templates which give the smallest rms values, whereas the second term favours those removing the least number of outliers. The balance between these two terms generally yields an automatic selection of the best templates that is in agreement with the visual inspection of the fitting procedure. Values of G in the interval 100–10 000 generally mean good fit, and, in absolute terms, also good light curve with small scatter (Ripepi et al. 2016). On the contrary, values of G below 100 are usually associated with highly scattered light curves. Finally, we retained only sources with the G parameter between 100 and 10 000 and K_s-band amplitude ≥ 0.04 mag further reducing the sample to 3636 best candidates with $\langle K_s \rangle$ magnitude in the range of 12.31–18.21 mag. This number appears to be still rather large if compared to expectations from the SFH recovery. A check was made by comparing the distributions of CCs in the VMC tiles partially covered by OGLE III. In particular, half of the tile SMC 4_5 is covered by both OGLE III and VMC and the other half only by VMC (see Figs 1 and 5). We divided the tile into four subregions, each of them approximately covering the same area. The two western subregions lie within the OGLE III footprint, while the two eastern ones lie outside. OGLE III detected 53 CCs in the north-western subregion and 30 in the southern one. From the SFH performed by Rubele et al. (2015) and the theoretical ISs (Bono et al. 2000, 2001a,b), we obtain a total number of about 55 (with a minimum of 35 and a maximum of 76) CCs from the SFH recovery, in good agreement with the OGLE III findings. Our number of CC candidates in the two eastern subregions of tile SMC 4_5 is roughly 10 times that observed by OGLE III in the two western ones. This test suggests that the majority of the 3636 new candidate variable stars are not CCs and that a high level of contamination must be present among them. In particular there could be contamination by other types of variables, but also issues such as saturation (on the bright side), limiting magnitude and photometric error problems (on the faint side), blending effects, intrinsic problems of the NIR data, etc. These issues may particularly affect faint sources, thus leading to an overestimate of the number of variable sources. Indeed, the sample of 3636 new candidate variables includes 1677 sources with $\langle K_s \rangle < 17.0$ mag and 1959 fainter sources with $17.0 \leq \langle K_s \rangle \leq 18.2$ mag. However, according to the discussion in Section 3.1, only 2 per cent of the SMC CCs have $\langle K_s \rangle$ magnitudes fainter than 17.0 mag. Hence, the 1959 candidate variables fainter than 17.0 mag should include, at most, ~ 40 bona fide CCs. We hence visually inspected only the K_s light curves of all 1677 sources brighter than $\langle K_s \rangle = 17.0$ mag and selected among them 297 sources whose K_s-band light curves have the typical shapes of CCs. In particular, all sources with very poor light-curve coverage were discarded since a firm classification was not possible. Moreover, for several sources the light curves did not show the typical shape of Cepheids; these sources were discarded as well. During the visual inspection, a percentage reliability flag has been assigned to each source. This flag is 100 per cent for a source with (i) good phase coverage, (ii) good light-curve shape and (iii) good position in the PL, while its value diminishes according to issues related to one or more of the aforementioned

Downloaded from https://academic.oup.com/mnras/article/459/2/1687/2595101 by guest on 28 November 2020

Table 3. Information on the 299 Cepheids that we have identified in the SMC using only the near-infrared photometry of the VMC survey. Column 1: VMC-SMC-CEP ID; column 2: right ascension (RA, J2000); column 3: declination (Dec, J2000); column 4: number of K_s observations; column 5: period computed with SigSpec; column 6: K_s amplitude computed with the template-fitting procedure; column 7: intensity-averaged K_s magnitude computed with the template-fitting procedure; column 8: *VarClass* flag assigned by the VSA; column 9: variability type assigned in the present study, corresponding percentage reliability flag and specific comments, if any. The table is published in its entirety as Supporting Information online. A portion is shown here for guidance regarding its form and content.

VMC ID	RA (deg)	Dec (deg)	N_{K_s}	$P_{\rm SigSpec}$ (d)	AmpK_s (mag)	$\langle K_s \rangle$ (mag)	*VarClass*	*VarType* and comments
001	01:43:58.77	−71:50:09.7	18	8.896 56	0.06	12.350	0	75 per cent CC few points at min
002	01:43:15.53	−71:42:49.8	18	8.897 351	0.08	12.599	0	75 per cent CC few points at min
003	01:28:07.58	−72:48:52.1	18	12.523 67	0.27	12.758	1	100 per cent CC GCVS2347
004	01:24:25.35	−74:16:50.5	16	13.151 942	0.29	12.792	1	100 per cent CC GCVS2343
005	01:42:56.52	−71:18:46.0	18	9.122 673	0.05	12.885	0	75 per cent CC few points at min
006	01:38:18.83	−71:22:18.4	18	8.886 835	0.04	13.076	0	75 per cent CC few points at min
007	01:23:00.57	−74:22:16.8	16	9.752 387	0.21	13.182	1	100 per cent CC GCVS2337
008	01:38:00.64	−71:39:22.2	18	8.887 862	0.06	13.269	0	75 per cent CC few points at min
009	00:29:43.53	−71:33:21.0	17	8.371 283	0.06	13.470	0	100 per cent CC
010	01:13:25.40	−70:58:09.2	14	5.233 301	0.06	13.533	0	75 per cent CC few points at min

features, becoming 62 per cent for sources that are not confirmed to vary.

Then we also checked a subsample of 240 among the 1959 sources fainter than $\langle K_s \rangle = 17.0$ mag; this provided two additional sources with light curves typical of CCs. Particular attention was devoted to sources showing a K_s-band amplitude between 0.04 and 0.1 mag since at this level of amplitude it is hard to distinguish between real variable sources and spurious objects. We hence decided to keep only low amplitude sources with a good light-curve coverage and very clear shapes.

We consider this total sample of 299 candidate variable stars that passed the colour–magnitude and colour–colour diagrams, PL, template parameters selections and the visual inspection of the light curve as bona fide Cepheids. Out of 299, nine sources are in common with the General Catalog of Variable Stars (GCVS; Artyukhina et al. 1995), two (VMC-SMC-CEP-258 and 286) are ACs in common with Soszyński et al. (2015a), while 288 are new CCs identified in the present study. The new CCs have periods in the range from about 0.34 to 9.1 d and span the magnitude range $12.9 \leq \langle K_s \rangle \leq 17.6$ mag, and only two being fainter than 17.0 mag (see above). This number is well consistent with the predictions of Rubele et al. (2015) SFH recovery in these external regions of the SMC. In particular, of the 299 confirmed Cepheids, only 13 are located in the eastern subregions of tile SMC 4_5. In the same two subregions Rubele et al. (2015) SFH recovery leads to a total number of about 10 (with a minimum of 4 and a maximum of 20) CCs, in very good agreement with our findings.

Table 3 lists our 299 SMC Cepheids along with their RA, Dec (J2000) coordinates, the period obtained with SigSpec (for a discussion about the errors see Section 3.2), the K_s-band amplitude and the intensity-averaged K_s magnitude computed with the template-fitting procedure, the *VarClass* parameter attributed by the VSA and the variability type (*VarType*) assigned in the present study together with comments, if any, and the aforementioned percentage reliability flag. The last column of Table 3 also provides the GCVS identification number, whenever appropriate. The sources are ordered by increasing magnitude going from brighter to fainter objects. Their spatial distribution over the SMC is shown in Fig. 5 where they have been marked as red filled circles.

During the revision phase of this manuscript, Soszyński et al. (2015b) paper presenting CCs in the Magellanic Clouds was posted as a preprint on the ArXiv. The authors comment that they can counter-identify 278 sources out of the 299 Cepheids in our list (the remaining 21 fall in the inter-CCD gaps of their camera; Soszynski, private communication) and they confirm 35 of the SMC Cepheids we have identified in our study. They also say that most of the remaining objects from our list turned out to be constant or nearly constant in the optical bands. We have cross-matched our catalogue with Soszyński et al. (2015b) and find that indeed 36 (about 13 per cent) of our Cepheids are confirmed by OGLE IV, namely, the nine CCs in common with the GCVS, the two ACs also identified by Soszyński et al. (2015a) and 25 new CCs. This result is encouraging, since it confirms that our method is promising despite the limited number of data points and the intrinsically low amplitude of the VMC light curves. But it is also quite puzzling due to the low rate of optical confirmations, since our 299 bona fide Cepheids were selected not simply because of the light variation in the K_s band, but, more importantly, because they also fall in the colour–magnitude and colour–colour diagrams where OGLE III SMC bona fide Cepheids are found, and because they also follow the SMC Cepheid PL relation.

The K_s-band light curves of our 299 bona fide SMC Cepheids folded according to the period derived from the analysis with SigSpec, are shown in Fig. 7. We first display the nine CCs in common with the GCVS and the 25 new CCs discovered in our study and later confirmed also by OGLE IV; all other bona fide Cepheids (including the two ACs) follow. The light curves appear overall quite symmetrical and it is difficult with the VMC K_s-band data to identify features such as bumps. K_s time series data for all of them are provided in Table 4. Among the remarks in the last column of Table 3, 'few points at min/max' is used whenever the light curve is not homogeneously covered at minimum or maximum light. For some of these sources, we checked the light curve of nearby sources within 5 arcsec, to rule out unidentified photometric problems that might cause/mimic the light variation. They look flat suggesting that the variability of the sources identified as Cepheids is real, even for less well sampled light curves.

Finally, we recall that according to the results in Section 3.3 our technique enables recovery of about a 66 per cent of the true Cepheids that may occur in these external regions of the SMC and that bona fide Cepheids may also be present in the sample of about 2000 candidate variables fainter than $K_s = 17.0$ mag that were not analysed here. Therefore, there are likely additional Cepheids that we may have missed either because their SigSpec periods are

Downloaded from https://academic.oup.com/mnras/article/459/2/1687/2595101 by guest on 28 November 2020

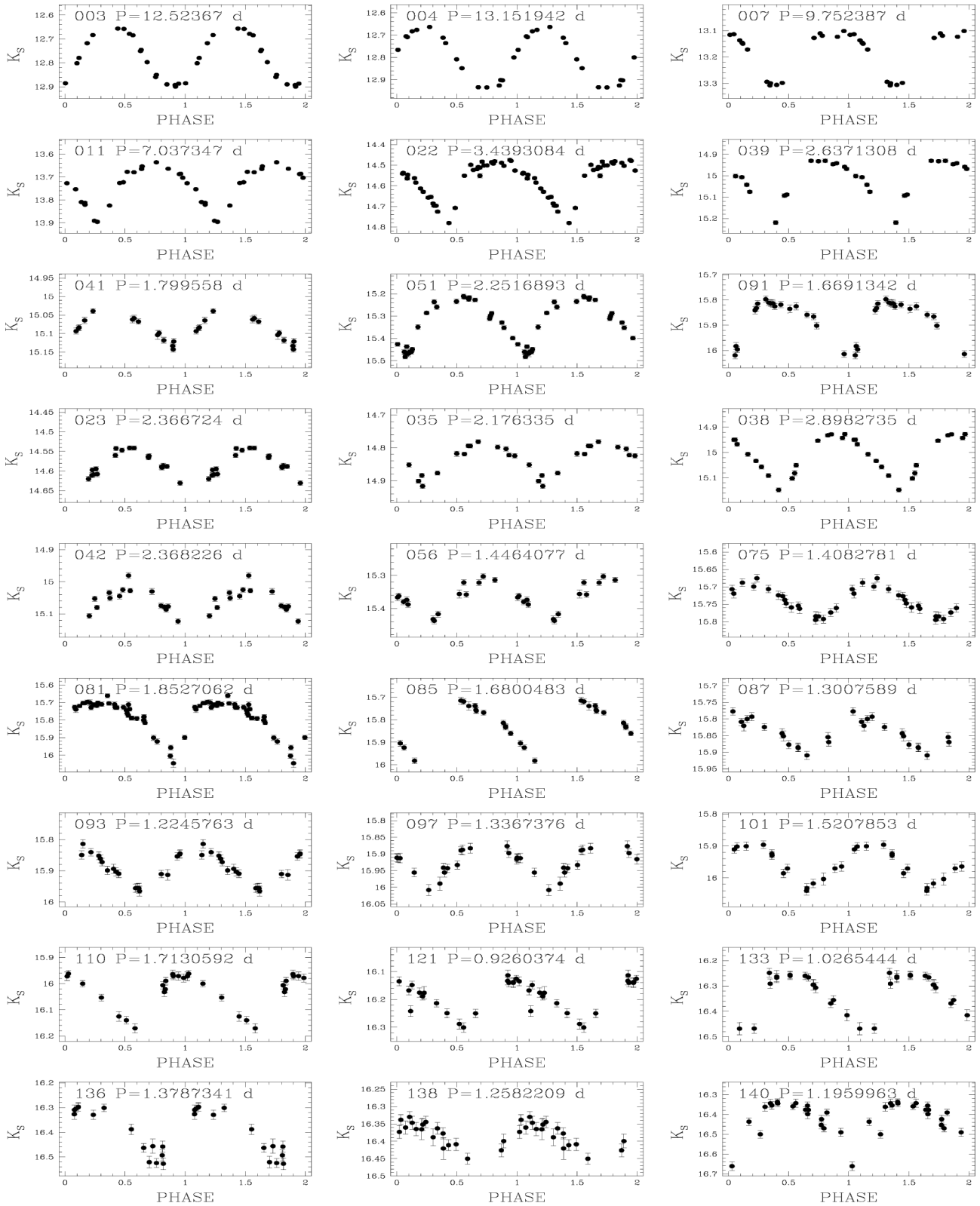

Figure 7. K_s-band light curves of bona fide Cepheids in the external regions of the SMC identified in the present study. For each source we indicate the VMC ID (ordered by increasing magnitude; see also Table 3) and the period derived from the analysis of the light curve with SigSpec. We first display the nine CCs in common with the GCVS (VMC-SMC-CEP-003, 004, 007, 011, 022, 039, 041, 051, 091) and 25 new CCs discovered in our study that were later confirmed also by OGLE IV (VMC-SMC-CEP-023, 035, 038, 042, 056, 075, 081, 085, 087, 093, 097, 101, 110, 121, 133, 136, 138, 140, 161, 166, 177, 188, 231, 237, 292). All other bona fide Cepheids (including the two ACs) follow. The figure is published in its entirety as Supporting Information online.

Downloaded from https://academic.oup.com/mnras/article/459/2/1687/2595101 by guest on 28 November 2020

Table 4. K_s-band time series photometry of our 299 SMC Cepheids. The table is published in its entirety as Supporting Information online. A portion is shown here for guidance regarding its form and content.

Star VMC-SMC-CEP-001		
HJD-2400000 (d)	K_s (mag)	errK_s (mag)
55834.792559	12.339	0.002
55927.600518	12.344	0.002
56146.865651	12.336	0.002
56147.757493	12.336	0.002
56155.743101	12.336	0.002
56159.787169	12.342	0.002
56163.761878	12.327	0.002
56175.694234	12.330	0.002
56188.672502	12.389	0.002
56189.703199	12.360	0.002
56190.724434	12.334	0.002
56208.619677	12.337	0.002
56226.551935	12.335	0.002
56256.553723	12.336	0.002
56282.578397	12.333	0.002
56300.546758	12.329	0.002
56486.866850	12.326	0.002
56911.795036	12.331	0.002

wrong by more than ±2.5 d, thus causing them to fall outside the 3σ boundaries of the PLs,[8] or because they are fainter than $K_s = 17.0$ mag.

4.1 Contamination by other types of variable stars

Adopting as reference the catalogue of RRLYR stars detected in the SMC by the OGLE III survey (Soszyński et al. 2010b), Muraveva et al. (in preparation) studied the K_s-band PL relation of 1081 SMC RRLYR stars observed by VMC. They found that these variables typically have K_s mean magnitude between 17.5 and 19.5 mag, with a subset of about 200 of them having $17.5 \leq \langle K_s \rangle \leq 18.2$ mag. In this magnitude range there is partial overlap with the short period, faint end of the CCs distribution (see Fig. 2). Furthermore, while the number of CCs is expected to drop significantly moving from the centre to the external region of the SMC, the distribution of RRLYR stars declines gently and their number is expected to remain rather high in the peripheral areas we are investigating (e.g. fig. 7 of Soszyński et al. 2015a). Therefore, some of the 1959 candidate variables with $17.0 \leq \langle K_s \rangle \leq 18.2$ mag may be RRLYR stars.

A further three percent contamination can also be expected from ECLs; they can spread all over the colour–magnitude diagram (see Moretti et al. 2014; Muraveva et al. 2014), thus we would need different criteria to distinguish them.

Finally, some of the sources could be ACs like VMC-SMC-CEP-258 and 286, or T2Ceps, due to the partial overlap existing among the PLs of the different types of Cepheids, especially between CCs and ACs (e.g. Soszyński et al. 2008b).

[8] Indeed, there are about 30 CCs detected by OGLE IV that are not in our list. These sources were not identified because their SigSpec period is incorrect (see Sections 3.2 and 3.3 for details); hence they did not pass the PL selection.

5 SUMMARY AND CONCLUSIONS

We have developed a technique to identify variable stars using only the multi-epoch near-infrared photometry obtained by the VMC survey and have specifically tailored it to the identification of Cepheids. The technique exploits colour–magnitude and colour–colour diagrams, and PL relations defined by known SMC Cepheids, along with template parameter selections and visual inspection of the light curve to identify bona fide Cepheids. The technique was applied to external regions of the SMC for which complete VMC K_s-band observations are available and no comprehensive identification of variable stars from other surveys exists yet. We have identified and present K_s-band light curves for 299 SMC Cepheids, of which nine are CCs in common with the GCVS (Artyukhina et al. 1995), two are ACs also found by Soszyński et al. (2015a) and the remaining 288 sources are new discoveries. The number of SMC Cepheids we have detected is consistent with the predictions of Rubele et al. (2015) SFH recovery in these regions of the SMC, taking into account that our technique may enable recovery of only about a 66 per cent of the true Cepheids that may occur in these external regions of the SMC. Subsequently, Soszyński et al. (2015b) cross-matched 278 of the sources in our list with their optical photometry and confirmed 36 of them as Cepheids. This result is encouraging, since it shows that our technique is promising despite the limited number of data points and the intrinsically low amplitude of the VMC light curves, but the low rate of optical confirmations is rather surprising and calls for further investigations to understand this discrepancy and possible physical/technical reasons behind it. This near-infrared versus optical light-curve connection/conspiracy will be addressed in a following paper.

ACKNOWLEDGEMENTS

This work is based on the observations collected at the European Organisation for Astronomical Research in the Southern Hemisphere under ESO programme(s) 179.B-2003. We thank the CASU and the WFAU for providing calibrated data products under the support of the Science and Technology Facility Council (STFC) in the UK. Partial financial support for this work was provided by PRIN-MIUR (2010LY5N2T) Chemical and dynamical evolution of the Milky Way and Local Group galaxies (PI: F. Matteucci) and PRIN-INAF 2014 EXCALIBURS: EXtra-galactic distance scale CALIBration Using first- Rank Standard candles. (PI: G. Clementini). We thank the anonymous referee for his/her constructive comments. RdG acknowledges funding support from the National Natural Science Foundation of China (grant 11373010). MIM thanks Felice Cusano and Alceste Bonanos for the interesting and useful discussions. M-RLC acknowledges support from the UK's Science and Technology Facilities Council [grant number ST/M001008/1] and from the German Academic Exchange Service.

REFERENCES

Alcock C. et al., 2000, ApJ, 542, 281
Artyukhina N. M. et al., 1995, General Catalogue of Variable Stars, 4rd ed., vol. V. Extragalactic Variable Stars, 'Kosmosinform'. Moscow
Bono G., Caputo F., Castellani V., Marconi M., 1999, ApJ, 512, 711
Bono G., Castellani V., Marconi M., 2000, ApJ, 529, 293
Bono G., Caputo F., Marconi M., 2001a, MNRAS, 325, 1353
Bono G., Gieren W. P., Marconi M., Fouqué P., 2001b, ApJ, 552, L141
Caputo F., Marconi M., Musella I., 2000, A&A, 354, 610
Castelli F., Gratton R. G., Kurucz R. L., 1997a, A&A, 318, 841
Castelli F., Gratton R. G., Kurucz R. L., 1997b, A&A, 324, 432

Downloaded from https://academic.oup.com/mnras/article/459/2/1687/2595101 by guest on 28 November 2020

Cioni M.-R. L. et al., 2011, A&A, 527, A116
Cioni M.-R. L. et al., 2013, The Messenger, 154, 23
Cross N. J. G., Collins R. S., Hambly N. C., Blake R. P., Read M. A., Sutorius E. T. W., Mann R. G., Williams P. M., 2009, MNRAS, 399, 1730
Cross N. J. G. et al., 2012, A&A, 548, A119
de Grijs R., Bono G., 2015, AJ, 149, 179
Emerson J., McPherson A., Sutherland W., 2006, The Messenger, 126, 41
Ferreira Lopes C. E., Cross N. J. G., 2016, A&A, 586, A36
Graczyk D. et al., 2011, Acta Astron., 61, 103
Haschke R., Grebel E. K., Duffau S., 2011, AJ, 141, 158
Haschke R., Grebel E. K., Duffau S., 2012, AJ, 144, 107
Kozłowski S. et al., 2013, Acta Astron., 63, 1
Kurtz D. W., 1985, MNRAS, 213, 773
Lewis J. R., Irwin M., Bunclark P., 2010, in Mizumoto Y., Morita K.-I., Ohishi M., eds, ASP Conf. Ser. Vol. 434, Astronomical Data Analysis Software and Systems XIX. Astron. Soc. Pac., San Francisco, p. 91
Marconi M., Musella I., Fiorentino G., 2005, ApJ, 632, 590
Moretti M. I. et al., 2014, MNRAS, 437, 2702
Muraveva T. et al., 2014, MNRAS, 443, 432
Muraveva T. et al., 2015, ApJ, 807, 127
Poleski R. et al., 2010, Acta Astron., 60, 1
Reegen P., 2004, in Zverko J., Ziznovsky J., Adelman S. J., Weiss W. W., eds, Proc. IAU Symp. 224, The A-Star Puzzle. Cambridge Univ. Press, Cambridge, p. 791
Reegen P., 2007, A&A, 467, 1353
Reegen P., 2011, Commun. Asteroseismology, 163, 3
Ripepi V., Moretti M. I., Clementini C., Marconi M., Cioni M. R., Marquette J. B., Tisserand P., 2012a, Ap&SS, 341, 51
Ripepi V. et al., 2012b, MNRAS, 424, 1807
Ripepi V. et al., 2014, MNRAS, 437, 2307
Ripepi V. et al., 2015, MNRAS, 446, 3034
Ripepi V. et al., 2016, ApJS, preprint (arXiv:1602.09005)
Rubele S. et al., 2012, A&A, 537, A106
Rubele S. et al., 2015, MNRAS, 449, 639
Soszyński I. et al., 2008a, Acta Astron., 58, 163
Soszyński I. et al., 2008b, Acta Astron., 58, 293
Soszyński I. et al., 2009a, Acta Astron., 59, 1
Soszyński I. et al., 2009b, Acta Astron., 59, 239
Soszyński I. et al., 2010a, Acta Astron., 60, 17
Soszyński I., Udalski A., Szymański M. K., Kubiak J., Pietrzyński G., Wyrzykowski Ł., Ulaczyk K., Poleski R., 2010b, Acta Astron., 60, 165
Soszyński I. et al., 2012, Acta Astron., 62, 219
Soszyński I. et al., 2015a, Acta Astron., 65, 233
Soszyński I. et al., 2015b, Acta Astron., 65, 297
Tisserand P. et al., 2007, A&A, 469, 387
Udalski A., Szymański M. K., Szymański G., 2015, Acta Astron., 65, 1
van der Marel R. P., Cioni M.-R. L., 2001, AJ, 122, 1807
Weldrake D. T. F., Sackett P. D., Bridges T. J., Freeman K. C., 2004, AJ, 128, 736

SUPPORTING INFORMATION

Additional Supporting Information may be found in the online version of this article:

Table 3. Information on the 299 Cepheids that we have identified in the SMC using only the near-infrared photometry of the VMC survey.
Table 4. K_s-band time series photometry of our 299 SMC Cepheids.
Figure 7. K_s-band light curves of bona fide Cepheids in the external regions of the SMC identified in the present study. For each source we indicate the VMC ID (ordered by increasing magnitude; see also Table 3) and the period derived from the analysis of the light curve with SigSpec.
(http://www.mnras.oxfordjournals.org/lookup/suppl/doi:10.1093/mnras/stw716/-/DC1).

Please note: Oxford University Press is not responsible for the content or functionality of any supporting materials supplied by the authors. Any queries (other than missing material) should be directed to the corresponding author for the article.

This paper has been typeset from a TEX/LATEX file prepared by the author.

Downloaded from https://academic.oup.com/mnras/article/459/2/1687/2595101 by guest on 28 November 2020